NASA Technical Memorandum 83804

Ceramic Microstructure and Adhesion

Donald H. Buckley
Lewis Research Center
Cleveland, Ohio

Prepared for the
Thirty-first National American Vacuum Society Symposium
Reno, Nevada, December 4–7, 1984

NASA

FINAL PROGRAM NUMBER
TE ThA03
(INVITED)
(put on JVST manuscript)

Ceramic Microstructure and Adhesion

Donald H. Buckley
National Aeronautics and Space Administration
Lewis Research Center
Cleveland, Ohio 44135

ABSTRACT

When a ceramic is brought into contact with a ceramic, a polymer, or a metal, strong bond forces can develop between the materials. The bonding forces will depend upon the state of the surfaces, cleanliness and the fundamental properties of the two solids, both surface and bulk. Adhesion between a ceramic and another solid are discussed from a theoretical consideration of the nature of the surfaces and experimentally by relating bond forces to the interface resulting from solid state contact. Surface properties of ceramics correlated with adhesion include, orientation, reconstruction and diffusion as well as the chemistry of the surface specie. Where a ceramic is in contact with a metal their interactive chemistry and bond strength is considered. Bulk properties examined include elastic and plastic behavior in the surficial regions, cohesive binding energies, crystal structures and crystallographic orientation. Materials examined with respect to interfacial adhesive interactions include silicon carbide, nickel-zinc ferrite, manganese-zinc ferrite, and aluminum oxide. The surfaces of the contacting solids are studied both in the atomic or molecularly clean state and in the presence of selected surface contaminants.

E-2311

INTRODUCTION

Ceramics like metals when in the atomically clean state will exhibit strong bonds of adhesion. This will occur for ceramics in contact with

themselves and other materials. There are a number of both bulk and surface properties of ceramics that will affect the nature and magnitude of the adhesive bond forces that develop for ceramics. With respect to surface properties these include electronic surface states, ionic species present at the surface, chemistry of the contacting material and the nature of surface contaminants present. Bulk properties include cyrstallography, cohesive binding energy and the presence or absence of defects.

When two solids are brought into contact and adhesion occurs there are a variety of methods which can be employed to quantify the bonding forces. Some involve tensile type pulling on the interface. Others are based upon tangential shearing of the junction. Friction force measurements are based upon the latter method. The stronger the interfacial bond strength the greater is the resistance to move one surface relative to the other tangentially. Such measurements are sufficiently sensitive that the effects of various fractions of an adsorbed monolayer on interfacial adhesion can be readily quantified (Ref. 1).

The objective of this paper is to review the fundamental properties of ceramics both surface and bulk and determine their influence on adhesive behavior. Ceramics to be examined, by way of example, will include silicon carbide, aluminum oxide, nickel-zinc ferrite, and manganese-zinc ferrite. The ceramics will be examined in contact with themselves, a polymer composite and with metals. Surface characterization will be used to establish surface states and the influence of films and contaminants.

RESULTS AND DISCUSSIONS

Oxide Ceramics

Oxides such as aluminum oxide, titanium oxide (rutile) and magnesium oxide have been considered for tribological applications. With these materials,

both structure and surface chemistry are extremely important to adhesion behavior.

Aluminum oxide. - In order to determine if friction and accordingly adhesion characteristics of sapphire were anisotropic, experiments in vacuum were conducted with two orientations of a sapphire ball. The first orientation involved the plane (0001) and the direction [11$\bar{2}$0] and the second the (10$\bar{1}$0) plane [0001] direction in adhesive contact and sliding against a disk of sapphire with its basal plane essentially parallel (within 4°) to the interface. The results obtained in these experiments are presented in Fig. 1 together with data for the (0001) plane and [11$\bar{2}$0] direction orientation examined in air to demonstrate the influence of adsorbed films.

The data of Fig. 1 indicates that the adhesion and friction characteristics of sapphire are highly anisotropic. At a moderate load of 0.25 N, the friction coefficient for the basal orientation was less than half that obtained for the prismatic orientation. As load is increased to 10 N both orientations show a decrease in friction coefficient. The marked differences in adhesion and friction for the two orientations are, however, maintained.

With metals, experiments conducted in vacuum serve to reduce the presence of adsorbed films and surface oxides. Sapphire has a layer of surface oxygen atoms as an inherent part of its structure, however adsorbed films may be removed on vacuum degassing. The differences in friction coefficients for the basal orientation of sapphire in air and at 10^{-8} Pa (Fig. 1) may be related to the influence of these films on the adhesion characteristics of sapphire.

The influence of crystallographic direction for both prismatic and basal orientations were determined and the results obtained are presented in Table I. With the basal orientation less adhesion and a lower coefficient of friction was observed in the preferred slip direction [11$\bar{2}$0]. This orientation

dependence is similar to that observed for the hexagonal metal berryllium in Ref. 1.

The crystallographic direction of movement on a surface, reflecting changes in atomic orientation also affect adhesion and friction force. This is demonstrated in the data of Table I for the prismatic and basal orientation of sapphire in contact with sapphire.

The results of Fig. 1 and Table I indicate that the adhesion and friction characteristics of sapphire are highly anisotropic. There was further, marked evidence for plastic deformation at the contacting interface of the crystals as revealed by etching of sapphire crystals after the friction experiments. The adhesion and friction behavior of sapphire in the figure and table is very analogous to that observed with hexagonal metals in Refs. 2 and 3. With hexagonal metals in sliding friction experiments the friction coefficient was always less on preferred slip planes in preferred slip directions than for other slip systems. Similar results were obtained in this investigation. The easy glide or slip plane for sapphire is the basal plane under deformation. Further the preferred slip direction is the $[11\bar{2}0]$ direction when the crystal is deformed plastically. With plastic deformation occurring at the contacting interface under an applied load it might be anticipated that the prismatic orientation of sapphire would exhibit stronger adhesion and higher coefficients of friction than the basal orientation. There are a number of prismatic planes which can slip in the deformation process while, with the basal plane oriented parallel to the sliding interface, only a single set of planes are involved.

When plastic deformation occurs at the sliding interface and a larger number of slip planes are involved, applied stresses in the form of the load may be distributed over a number of equivalent planes. With the basal plane

parallel to the sliding interface, any applied normal load can only tend to compress basal planes and even with metals such as beryllium, this orientation will support tremendous loads to the point where it will literally explode with no evidence of slip occurring on other slip planes. A larger true contact area can then occur in the sliding process with prismatic than with basal orientation. Further, when a number of prismatic planes undergo slip, there exists the possible interaction of such slip planes to produce locks similar to the Lomer-Cottrell locks observed in the face centered cubic metals. Such locks can produce marked increases in shear strength.

With sapphire the yield point for the prismatic orientation is different than that for the basal orientation. For the latter orientation the yield stress is ten times less at elevated temperatures (Ref. 5).

The shear strength for sapphire calculated from adhesion and friction measurements of this investigation together with bulk shear strength data obtained from Ref. 4 are presented in Table II. The surface shear strength is from twenty to thirty times that of the bulk shear strength. Similar results have been observed with a number of inorganic crystals in Ref. 4. A possible explanation for this increase may be that indicated in Ref. 5. Microscopic plastic deformation occurring at the sliding interface permits relief of stresses in the sapphire resulting in an increase in shear strength.

The authors of Refs. 6 to 13 were all concerned with the influence of orientation on adhesion, friction and/or most frequently wear. The experiments of these investigators were all conducted at higher speeds than employed in this investigation. Loads, however, in many instances were lighter than employed in this study. It should be indicated that interfaces temperatures in a vacuum environment may be considerably higher than is encountered air under equivalent conditions of load and speed because of poor heat

dissipation. Further, higher coefficients of friction in vacuum for sapphire (Fig. 1) will further increase interface temperatures. For example, increases in adhesion and friction observed in this study at 500° C was not observed in shear strength measurements of Ref. 14 until temperatures of approximately 1000° C. Some surface contaminants such as chlorine are not fully removed below 1000° C.

Data of Ref. 3 showed the recrystallization of titanium metal at a 500 g load and the same speed as employed in this study. Titanium would normally recrystallize in the temperature ranges of plastic deformation discussed here for sapphire. It is therefore reasonable to assume plastic deformation for aluminum oxide under similiar load conditions.

The lower coefficient of friction measured for the basal orientation of sapphire sliding on sapphire in Fig. 1 are as might be predicted from observed slip behavior. In plastic deformation experiments of Ref. 14 very little resolved shear stress was necessary to initiate slip on basal planes while the shearing stress for prismatic slip was at the maximum.

In this study, adhesion at the sliding interface with the prismatic orientations resulted in prismatic slip. With hexagonal metals such as cobalt orientation of single crystals for prismatic slip results in slip plane and slip plane dislocation interaction, strain hardening and consequently increase in measured friction. Cross slip mechanisms which can account for strain hardening in metals must be modified for sapphire since only two slip systems operate. Cross slip on the same system may not be possible but prismatic plane dislocations can interact with stacking faults of the basal planes producing strain-hardening. Ref. 14 referred to strain hardening for prismatic slip in sapphire. This interaction of basal stacking faults cannot occur for the basal slip mechanism because the basal dislocations and stacking faults

lie in the same plane. The adhesion and friction data of this investigation indicate, as did the wear data of Ref. 6, that plastic deformation dictates the adhesion and sliding behavior of sapphire.

When oxide ceramics are in solid state contact with softer materials such as metals the marked difference in elastic and plastic deformation of the two materials can result in considerable plastic deformation of the softer material. This can contribute to the adhesion of the materials because it increases real contact area. In Fig. 2 a rider (hemisphere) of sapphire slid on a single crystal flat of copper. The specimen materials were then reversed so that a single crystal copper rider slid on a sapphire flat. The coefficient of friction for the sapphire sliding on copper was 1.5. With copper sliding on sapphire, it was 0.2. In both instances, adhesion of copper to sapphire occurred. The difference in friction coefficient for the two experiments is due to the effects of plowing or plastic deformation of the copper. Plowing of the copper disk, which did not occur with the sapphire disk contributed heavily to measured friction.

Also in both experiments the sapphire adhered to the copper as indicated in the photomicrographs of Fig. 2. The wear on the sapphire flat was occasioned by fracture along (0001) planes and subsurface and parallel to the sliding interface. When metals contact oxide ceramics, surface chemistry plays a very important role in the observed adhesion and friction behavior. Various metals were slid on a flat of sapphire with the basal orientation in the sapphire parallel to the sliding interface. With the metals which form stable oxides such as copper, nickel, rhenium, cobalt and beryllium, adhesion of the metal occurred to the oxygen ions in the outermost atomic layer of the sapphire. The manner of bonding is shown in Fig. 3.

When the same sliding experiments are conducted with metals that do not form stable oxides in vacuum (gold and silver) strong chemical bonding does

not occur at the interface, adhesion is weak and wear to the hard oxide ceramic is absent. This is demonstrated in the data of Fig. 4 for gold and silver sliding on the basal orientation of sapphire.

The photomicrographs of Fig. 4 indicate an absence of any wear to the sapphire such as observed in Fig. 2 with copper. The only surface markings in Fig. 4 were polishing scratches. The coefficients of friction were also one-half in Fig. 4 of that observed with copper in contact with sapphire in Fig. 2. In Fig. 2 fracture occurred with adhesion in the sapphire because the interfacial metal to the sapphire bond strength is greater than the cleavage or fracture strength in the sapphire and accordingly sapphire fracture occurs. With gold and silver in Fig. 4, the weakest region is the interface and simple shear takes place at this location with bond strength no stronger than found with lubricant molecules as evidenced by the friction coefficient of 0.1 comparable to that experienced with effective boundary lubrication.

Experiments subsequent to those herein confirmed a chemical bond between metals and the oxygen ions indicated in Fig. 3 (Ref. 15). The shear strength of the metal to sapphire contact were correlated with the free energy of formation of the metal oxide in Ref. 15.

Further attempts have been made to explain in a more fundamental manner the metal to sapphire bonding. This could assist in understanding the wear of hard ceramic oxides in general. Molecular-orbital energies have been examined for clusters in bulk sapphire and the metal-sapphire interface (Ref. 16).

Ferrites. - With oxide ceramic materials such as Mn-Zn and Ni-Zn ferrites adsorbates are present on the surface from the environment, and these include water vapor and carbon, as typically shown in Fig. 5(a). With metals, in addition to the presence of adsorbate films, beneath this layer of adsorbate is generally a layer of metal oxide.

The adsorbed films on ferrites and metals as well as oxides on metals can generally be removed by sputtering or heating. For example, in Fig. 5(a) the adsorbates have disappeared from the spectrum taken after sputter-cleaning. In addition to oxygen and iron, which are associated with the composition of Mn-Zn ferrite, the XPS peaks obtained from the sputter cleaned surface indicate manganese and zinc, but there is no adsorbate.

The adsorbates play a very large role in adhesion, mechanical and chemical behavior of ferrite surfaces in tribological systems. Experiments carried out in two environments, vacuum and argon at atmospheric pressure indicate the effects of adsorbate and environment on adhesion and friction properties. The removal of adsorbed films from the surfaces results in very strong interfacial adhesion and high friction.

The data obtained from the experiments in vacuum are to be anticipated from chemical interactions and the important role they play in the adhesion and friction of clean ferrite-to-metal couples. The behavior is analagous to that observed for aluminum oxide.

The coefficients of friction reflecting interfacial adhesion for various metals sliding on ferrites in argon atmosphere were all nearly 0.1 to 0.2. The chemical activity or inactivity of metal does not appear to play a role as to adhesion and friction in argon as the argon is only physically adsorbed. A prerequisite for this sameness in friction is that the metals form a stable metal oxide, and the environment is responsible for providing the adsorbates on the surface.

Similiar exper ments with ferrites contacting polymeric magnetic indicate that adsorbed nitrogen will appreciably reduce adhesion and accordingly friction. Oxygen conversely increases adhesion and friction.

The adhesion and accordingly coefficients of friction for polycrystalline Ni-Zn and Mn-Zn ferrite in contact with metals can be correlated with the free

energy of formation of the lowest metal oxides, as shown in Fig. 6. The correlation shown in Fig. 6 clearly indicates that the metal-ferrite adhesive bond at the interface is primarily a chemical bond between the metal atoms and the large oxygen anions in the ferrite surface, and the strength of this bond is related to oxygen to metal bond strength in the metal oxide (Ref. 17.).

All metals indicated in Fig. 6 adhered and transferred to the surface of the ferrites. In general the less active the metal, the less adhesion and transfer there is to the ferrite. Titanium, having a much stronger chemical affinity to the elements of the ferrite, exhibited the greatest amount of transfer (Ref. 18).

The relative chemical activity of the transition metals (metals with partially filled d shells) as a group can be ascertained from their percentage d-bond character, as established by Pauling (Ref. 19). The frictional properties of metal-metal and metal-nonmetal contacts have been shown to be related to this character (Ref. 20 to 23). The greater the percentage of d-bond character, the less active is the metal, and the lower is the adhesion and friction. Conversely, the more active the metal, the greater is the adhesion.

The coefficients of friction for various metals in contact with Ni-Zn ferrites are replotted with solid symbols in Fig. 7 as a function of the d-bond character of the transition metal. Titanium, which is a chemically active metal, exhibits a considerably higher coefficient of friction in contact with ferrite than does rhodium, which is a metal of lesser activity.

Figure 7 also presents the coefficient of friction for various metals in contact with the ferrites, in which both metal and ferrite specimens were exposed to O_2 gas (99.99 percent pure). The data reveal increase in adhesion and the coefficients of friction for Ni-Zn ferrite-to-metal interface.

The enhanced bond of the metal oxide to ferrite may be due to the formation of complex oxides on establishing contacts.

Figure 8 presents the coefficients of friction for various magnetic tapes in contact with ferrites as a function of particle loading in vacuum. For the experiments in vacuum the specimens were placed in the vacuum chamber, and the system was evacuated and baked out to achieve a pressure of 30 nPa (10^{-10} torr). The ferrite specimen was then ion-sputter cleaned. The data shown with solid symbols in Fig. 8 presents the coefficients of friction for the tapes sliding against sputter cleaned ferrite. Sliding friction experiments were also conducted with ferrite specimens, which were first argon-ion sputter cleaned, exposed to 1000 L oxygen, and then were brought into contact with magnetic tapes in the system reevacuated to a pressure of 30 nPa (10^{-10} torr). These results are presented in Fig. 8 with open symbols.

The data of Fig. 8 reveal that the adsorption of oxygen on polymeric magnetic tape and on sputter cleaned ferrite surfaces increases adhesion and the coefficients of friction for ferrite-to-magnetic tape interfaces. The oxygen exposures did strengthen the ferrite-to-tape adhesion and increased friction. The coefficient of friction is also strongly dependent on the particle loading. The greater the magnetic particle concentration (particle loading), the lower the coefficient of friction.

NONOXIDE CERAMICS

The high strength and excellent oxidation and creep resistance of nonoxide ceramics such as silicon carbide make them extremely important materials for high-temperature mechanical and electronic applications in severe environments. Materials such as silicon carbide are used for example, in stable high-temperature semiconductors, in gas turbine blades, in turbine ceramic seals, and as an abrasive for grinding (Refs. 24 and 25).

In grinding, as a result of the extremely small chip size and the high wheel speed involved, the instantaneous temperatures and pressures at the tip of a silicon carbide abrasive particle are extremely high (Ref. 26). The temperature and pressure may reach the melting point and the yield pressure of the metal workpiece. In addition, the freshly formed surfaces of silicon carbide are highly reactive with metals. The fundamentals of the surface chemistry involved in adhesion, and tribological properties of silicon carbide are not clearly understood.

Experimental work has been conducted at room temperature to gain an understanding of the surface of silicon carbide and its adhesion and friction properties (Refs. 27 and 28). These properties depend strongly on the surface characteristics of silicon carbide. In turn the surface characteristics of silicon carbide are strongly affected by temperature. For example, an increase in temperature in vacuum can cause graphitization of the carbon and depletion (by evaporation) of the silicon. The adhesion and tribological behavior of silicon carbide at high temperatures in vacuum is therefore important. The knowledge gained from such studies can assist in achieving a better understanding of the surfaces characteristics of silicon carbide when in solid state contact with other materials.

Tribological properties involve the adhesion, friction and wear of the silicon carbide and the metal transfer to the silicon carbide. Surfaces of silicon carbide were heated to 1500° C in a vacuum at a pressure of 10 nPa by resistance heating and then the surfaces were analyzed at room temperature. The surface chemistry of silicon carbide crystals was analyzed by X-ray Photoelectron Spectroscopy (XPS) as well as Auger Electron Spectroscopy (AES).

AES analysis of silicon carbide preheated above 1200° C indicated that the silicon AES peak had almost disappeared and was nearly undetectable by AES,

and the carbon peak was only of the graphite form at the surface. But XPS analysis clearly indicated that evidence for silicon and carbide being present as well as graphite on the silicon carbide surface preheated above 1200° C. The XPS spectra of the silicon carbide surface was uneffected by preheating in the temperature range of from 1200° to 1500° C.

A depth profile into the surface layers for elements present in silicon carbide surface preheated to 1500° C was obtained as a function of sputtering time and is presented in Figure 9. The graphite peak decreases rapidly in the first 30 minutes of sputtering, and thereafter it gradually decreases with an increase in the sputtering time to about 18 hr. After 18 hr the graphite peak does not change much with sputtering time. On the otherhand, the silicon and carbide-carbon peaks increase gradually with increasing sputtering time to 20 hr.

Ellipsometeric measurements have been conducted with two different (0001) faces of the silicon carbide crystals, one which consisted of silicon atoms (0001) and the other which consisted of carbon atoms (0001) at temperatures above 1200° C (Ref. 29). In one hour of heating at 1300° C the layer, which consists of carbon (graphite), on the C-face grows to about 100 nm, whereas the layer on the Si-face did not grow thicker than 10 nm even with longer heating.

The silicon carbide $\{0001\}$ surfaces used in this investigation consisted of both silicon atoms and carbon atoms because etching silicon carbide surface in molten salt $1NaF + 2KCO_3$ gives both a smooth surface for the Si-face and a rough one for the C-face. The apparent thickness of the layer, which consists of graphite at the surface and is produced by heating above 1200° C for 1 hr, is about 100 nm (1000 Å), and it is equivalent to a depth of a layer sputter etched for about 18 hr shown in Fig. 9.

The graphitization of the outermost surficial layer of silicon carbide is believed to be as follows. The analysis depth with AES is of the order of 1 nm or less and an elemental concentration as low as 0.1 percent of a monolayer can be detected and identified. Therefore, the outermost surficial layer, which consists of mostly graphite and very little silicon, on the silicon carbide surface is concluded to be of the order of 1 nm. This estimation is consistent with the proposition of Bommel, et al. (Ref. 30), that is the collapse of the carbon of three successive silicon carbide layers is the most probable mechanism for the initial stages of the graphitization of silicon carbide basal planes.

Adhesion and sliding friction experiments were conducted with single-crystal silicon carbide in contact with iron in vacuum. Friction-force traces resulting from such sliding were generally characterized by strong adhesion and a stick-slip behavior. All the coefficients of friction reported in Fig. 10 are static values reflecting adhesion forces at the interface. The coefficent of static friction is defined as: $\mu_s = F_1/W$, where F_1 is the friction force at which the first break, in adhesion occurs, that is, first motion is observed in the friction-force trace and W is the normal load.

The coefficient of friction of the silicon carbide $\{0001\}$ surfaces in contact with iron as a function of sliding temperatures is indicated in the graph of Fig. 10. The iron rider was sputter cleaned with argon ions. The silicon carbide was in the as-received state after it had been baked out in the vacuum system. The specimen was then heated to the sliding temperature before the friction experiment was initiated. The coefficient of friction increased slightly with increasing temperature at temperatures below 400° C. Above 400° C, the coefficient of friction decreased with an increase in

temperature in the range of 400° to 600° C. The general decrease in friction at these temperatures is due to the gradual removal of the contaminants of carbon and oxygen from the surface. This is in contrast to metals where removal of surface films increases friction. The coefficient of friction increased with increasing temperature in the range of 600° to 800° C. The increase in friction at the temperature can be associated with increased adhesion and increased plastic flow in the area of contact. Above 800° C the coefficient of friction decreases rapidly with an increase of temperature. The rapid decrease in friction above 800° C correlated with the graphitization of the silicon carbide surface.

Inspection of the single-crystal silicon carbide surface after sliding contact with iron revealed adhesion and transfer of iron to silicon carbide. Fig. 11 shows scanning electron micrographs at beginning the of wear tracks on the as-received and treated surfaces of silicon carbide generated by a single pass of the iron at sliding temperatures of room, 800° and 1200° C. It is obvious from Fig. 11 the copious amount of iron adhered and transferred to the silicon carbide. The increase in friction at these higher temperatures can be associated with increased adhesion and increased plastic flow in the area of contact. Above 800° C the coefficient of friction decreases rapidly with an increase of temperature. The rapid decrease in friction above 800° C correlated with the graphitization of the silicon carbide surface.

Iron undergoes the crystal transformation from BCC to FCC at 912° C but this does not account for observed friction behavior. Similiar experiments with rhodium metal, where a transformation does not occur gave similiar friction.

Inspection of the single-crystal silicon carbide surface after sliding contact with iron revealed adhesion and transfer of iron to silicon carbide.

Figure 11 shows scanning electron micrographs at beginning of wear tracks on the as-received and treated surfaces of silicon carbide generated by a single pass of the iron at sliding temperatures of room, 800° and 1200° C. It is obvious from Fig. 11 that the copious amount of iron adhered and transferred to the silicon carbide. As may be seen in Fig. 1(a), sliding at 800° C produces more transfer than does sliding at room temperature. In general, a very thin transfer film and very small particles are seen in the contact area. The higher the sliding temperature, the more adhesive transfer produced. Above 800° C, there was very little evidence for a smooth and continuous adhered transfer film on the wear track, as typically seen in Fig. 11(c). There was rather transfer that was rough, and discontinuous in nature. The appearance of iron transfer may be related to the graphite layer, of the order of to 1 nm, on the silicon carbide surface.

The adhesion and sliding of iron on a silicon carbide surface at elevated temperatures results in formation of cracks and fracture pits in the silicon carbide surface. The fracture wear occurs very locally and in very small areas in the sliding contact region.

Figure 12 presents scanning electron micrographs of the wear track on the silicon carbide surface, where the wear track is generated by a single-pass sliding of the iron rider. The wear track has in it microfracture pits and debris resulting from adhesion. Two kinds of fracture pits are generally clearly observed in the wear track: (1) pit with a spherical particle, and (2) pit with a multiangular shaped wear debris particles having crystallographically oriented sharp edges and which are nearly all of a platelet hexagonal shape.

Such multiangular wear debris are generated by surface cracking along $\{10\bar{1}0\}$ or $\{11\bar{2}0\}$ and the sub-surface cracking long (0001) planes, which

are parallel to the sliding interface. It is understandable that the fracturing in the single crystal of silicon carbide is characterized by crystallographic orientation. However, the appearance of fracture pits with a spherical shape is an interesting observation.

Various fracture pits with spherical particles were observed in the very local area of wear tracks. It was found in Ref. 22 that spherical wear particles of silicon carbide are observed as a result of sliding friction experiments with iron binary alloys. A mechanism for the generation of fracture pit with a spherical particle seems to be very similar to that of spherical wear particles described in Ref. 22.

Two possible mechanisms for the generation and formation of the spherical wear debris particles were described: (1) a penny-shaped crack along the circular stress trajectories and (2) an attrition of wear particles. However, the second mechanism is not applied to the fracture pit with the spherical particles. The possible mechanism is the first one, that is, the penny-shaped cracking. The details of the penny-shaped fracture mechanism was described in Ref. 21. Briefly stated, the stress trajectories under the point contact loading at the interface is similar to the Hertzian field (Ref. 22). The stress concentration acts in very small contact region and produces a small zone of inelastic deformation. This deformation will induce the generation and propagation of cracks. The cracks will suddenly initiate at locations of pre-existing flaw, almost certainly at the surface just outside the stress concentrated contact area where the contours of greatest principal tensile stress exist during sliding. A cracking mechanism is therefore the sudden development of a penny-shaped crack along the circular stress trajectories produced.

Sliding of iron on a silicon carbide surface results in both the transfer of iron to silicon carbide and very occasionally a transfer of silicon carbide

wear debris on the iron rider. Above 400° C, graphite produced on the silicon carbide surface transfers to the iron pin during sliding contacts.

SUMMARY REMARKS

The adhesion behavior of ceramics in contact with themselves, metals and polymers is strongly dependent upon the chemistry of the ceramic surface and that of the solids with which contact is made. With clean ceramic surfaces in contact crystallographic orientation influences adhesion as determined by friction force measurements. Friction force measurements are especially effective in gaining quantitative information on interfacial bond strengths.

Ceramics, just as has been observed with metals, exhibit the smallest adhesive bond forces and accordingly the lowest friction for the high atomic density low surface energy crystallographic planes. This has been observed with oxide ceramics such as aluminum oxide and nonoxide ceramics such as silicon carbide.

With ceramics in contact with polymeric materials such as magnetic tapes environment is extremely important. For example, with the ferrites contacting polymeric tapes adsorption of nitrogen on the surface will appreciably reduce adhesion of the polymeric structure to the ferrite ceramic while the adsorption of oxygen will appreciably increase adhesion and measured friction forces.

When metals are in contact with ferrites (Ni-Zn and Mn-Zn ferrites) the adhesion and friction behavior can be related to the d valence bond character of the metals. The greater tha percent bond saturation, the lower is the adhesion and friction for the metals in contact with the ferrites. Similarly, the adhesion and friction can be related to the free energy of formation of the lowest metal oxide. The less the energy, the lower the adhesive and frictional bond forces. Again, as with polymer, exposure to oxygen results in an increase in adhesive bond strength. It appears that oxygen acts, as it were, as an adhesive for these contacts.

For metals contacting aluminum oxide again the chemical activity of the metal is important to adhesive behavior. With noble metals silver and gold interfacial adhesive bonds were sufficiently weak so as not to result on separation of damage to the surfaces of the contacting solids. With other metals that form stable oxides the interfacial adhesive bonds were sufficiently strong so as to result in fracture of single crystal sapphire when cleavage planes were parallel to the contact interface. Metals undergo shear when the ceramic is polycrystalline aluminum oxide and attempts are made to, by tangential motion to fracture the adhered interface. Adsorbates reduce significantly adhesion and friction forces.

With the nonoxide ceramic, silicon carbide, heating to temperatures above 800° C results in reconstruction of the surface with the formation of graphite. The graphite reduces adhesion. Just as with oxide ceramics metals whose surfaces are chemically active bond very strongly to the silicon carbide. The interfacial bond strength is generally stronger than the cohesive bonds in the metal and metal will transfer to the silicon carbide. Under certain conditions, however, fracture will occur in the silicon carbide on separation. It can follow crystallography yielding hexagonal shaped fracture pits on the basal plane of alpha silicon carbide or completely ignore orientation and produce spherically shaped pits completely independent of crystal structure.

REFERENCES

1. D. H. Buckley, Surface Effects in Adhesion, Friction, Wear and Lubrication (Elsevier, Amsterdam, 1981).
2. D. H. Buckley, "Effect of Orientation on Friction Characteristics of Single-Crystal Beryllium in Vacuum (10^{-10} torr)," NASA TN-D-3485, July 1966.
3. D. H. Buckley, "Influence of Crystal Orientation on Friction Characteristics of Titanium Single Crystals in Vacuum," NASA TN-D-2988, Sept. 1965.

4. R. F. King and D. Tabor, Proc. R. Soc. London, Ser. A, 223, pp. 225-238 (1954).

5. J. B. Wachtman Jr. and L. H. Maxwell, Am. Ceram. Soc. J., 42 432-433 (1959); see also W. D. Kingery, H. K. Bowen and D. R. Uhlmann, Introduction to Ceramics, (Wiley, New York, 1976), 2nd ed.

6. R. P. Steijn, J. Appl. Phys., 32 1951-1959 (1961).

7. E. J. Duwell, J. Appl. Phys., 33 2691-2698 (1962).

8. C. H. Riesz, "Mechanisms of Wear of Nonmetallic Materials, "WADC-TR-59-316, Pt. II, May 1960.

9. C. H. Riesz and H. S. Weber, "Mechanism of Wear of Nonmetallic Materials," WADC-TR-59-316, Pt. III, February 1962.

10. E. J. Duwell and H. C. Butzke, ASLE Trans., 7 101-108 (1964).

11. E. J. Duwell and H. E. Butzke, J. Appl. Phys., 35 3385-3390 (1964).

12. W. R. Brown, N. S. Eiss Jr. and H. T. McAdams, Am. Ceram. Soc. J., 47 157-162 (1964).

13. A. G. King, Am. Ceram. Soc. Bull., 43 395-401 (1964).

14. R. Scheuplein and P. Gibbs, Am. Ceram. Soc. J., 45 439-452 (1962).

15. S. V. Pepper, J. Appl. Phys., 47 (3) 801-808 (1976).

16. K. H. Johnson and S. V. Pepper, J. Appl. Phys., 53 (10) 6634-6637 (1982).

17. K. Miyoshi and D. H. Buckley, "Properties of Ferrites Important to Their Friction and Wear Behavior," NASA TM-83718, 1984.

18. K. Miyoshi and D. H. Buckley, Wear, 66 157-173 (1981).

19. L. Pauling, Proc. R. Soc. London, Ser. A, 196 343-362 (1949).

20. D. H. Buckley, J. Colloid Interface Sci., 58 36-53 (1977).

21. K. Miyoshi and D. H. Buckley, Appl. Surf. Sci., 6 161-172 (1980).

22. K. Miyoshi and D. H. Buckley, ASLE Trans., 22 245-256 (1979).

23. D. H. Buckley, ASLE Trans., 21 118-124 (1978).

24. Silicon Carbide, a High Temperature Semiconductor, edited by J. R. O'Connor and J. Smiltens (Pergamon, New York, 1960).

25. R. C. Marshall, J. W. Faust Jr., and C. E. Ryan, Silicon Carbide - 1973; Proc. of the Third International Conference, (Univ. of South Carolina Press, Columbia 1974).

26. R. Komanduri and M. C. Shaw, J. Eng. Ind., 98 (4) 1125-1134 (1976).

27. K. Miyoshi and D. H. Buckley, ASLE Trans., 22 (3) 245-256 (1979).

28. K. Miyoshi and D. H. Buckley, "Effect of Oxygen and Nitrogen Interactions on Friction of Single-Crystal Silicon Carbide," NASA TP-1265, July 1978.

29. F. Meyer and G. J. Loyen, Acta Electron, 18 33-38 (1975).

30. A. J. Van Bommel, J. E. Crombeen and A. Van Tooren, Surf. Sci., 48 (2) 463-472 (1975).

TABLE I. - THE INFLUENCE OF CRYSTALLOGRAPHIC DIRECTION ON THE COEFFICIENT OF FRICTION FOR SAPHIRE SLIDING ON SAPPHIRE IN VACUUM (30 nPa)

[Load, 10 N; sliding velocity, 0.013 cm/sec.]

Plane	Direction	Coefficient of friction
Prismatic $(10\bar{1}0)$	$[11\bar{2}0]$	0.93
	[0001]	1.00
Basal (0001)	$[11\bar{2}0]$	.50
	$[10\bar{1}0]$	.96

TABLE II. - BULK AND SURFACE SHEAR STRENGTH DATA FOR SAPPHIRE[a]

Source	Shear strength 1×10^6 N/m^2
Bulk shear strength	34.0
Surface shear strength from friction	
(0001) $[11\bar{2}0]$	680.0
$(10\bar{1}0)$ [0001]	1020.0

[a]Surface shear strengths calculated from friction values.

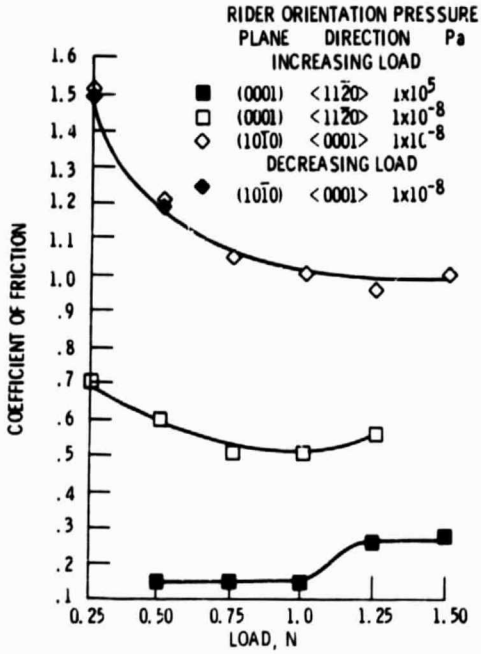

Figure 1. - Coefficient of friction as function of load for sapphire sliding on sapphire in vacuum, 30 nPa and air, 1x10^{5} Pa. Sliding velocity, 0.13 centimeter per second; temperature, 298 K; specimen outgassing with electron gun at 573 K. Disk specimen was (0001) plane parallel to sliding interface.

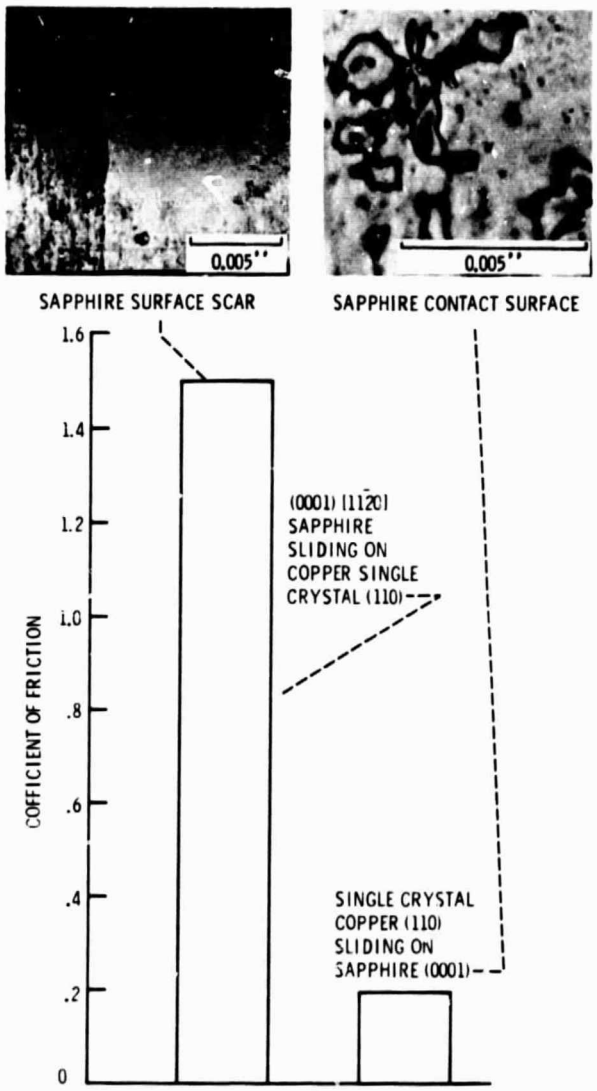

Figure 2. - Coefficient of friction for copper in sliding contact with sapphire in vacuum (30 nPa). Load, in sliding velocity, 0.013 centimeter per second.

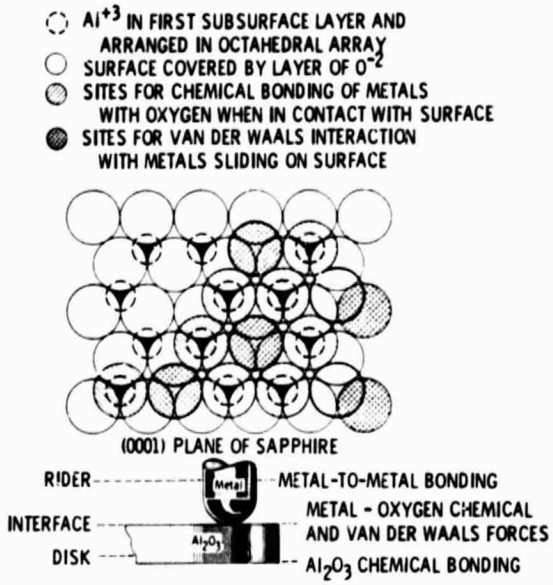

Figure 3. - Nature of surface interaction and bonding of metal to Al_2O_3.

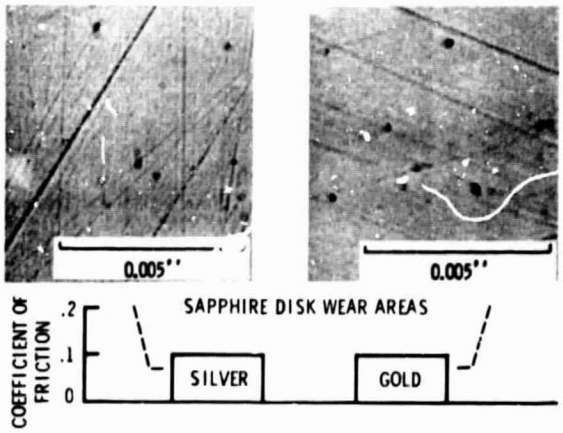

Figure 4. - Coefficient of friction for gold and silver riders sliding on sapphire in vacuum (30 nPa). Sliding velocity, 0.013 centimeter per second; ambient temperature, 298° K; duration, 1 hour.

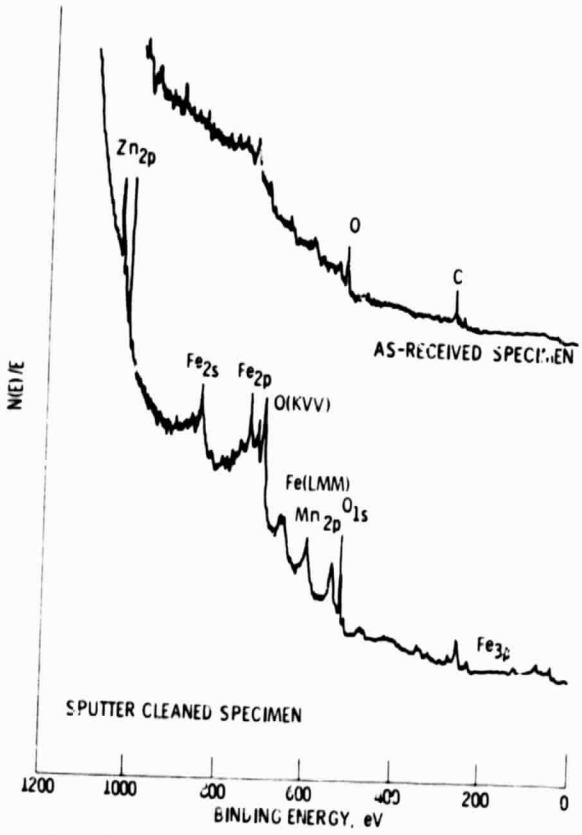

Figure 5. - XPS-survey spectra of the Mn-Zn-ferrite surfaces.

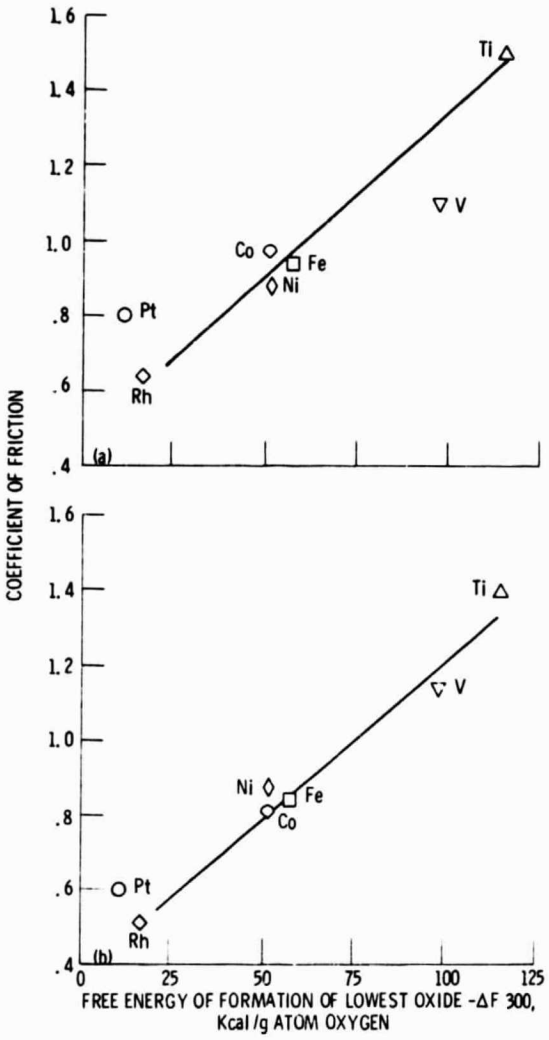

Figure 6. - Coefficients of friction for various metals in contact with (a) Ni-Zn and (b) Mn-Zn ferrites as a function of the free energy of formation of the lowest oxide. Single-pass sliding; sliding velocity, 3 mm/min; load, 0.05 to 0.2 N; vacuum, 30 nPa; room temperature.

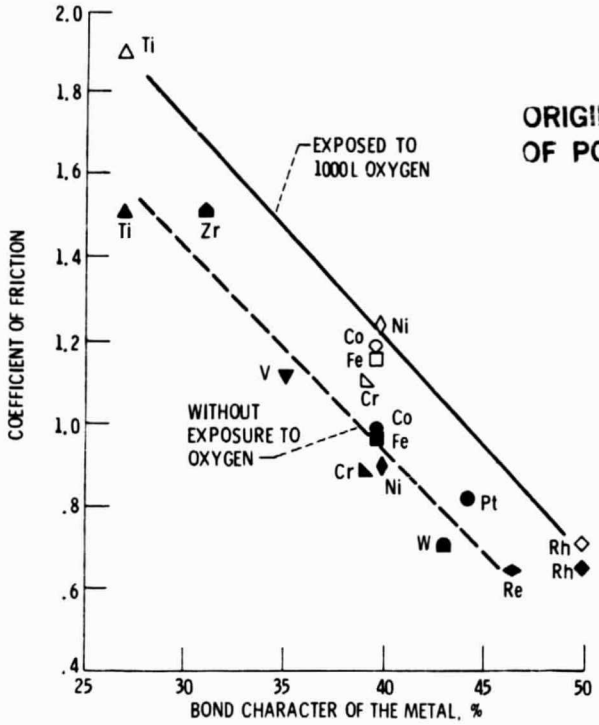

Figure 7. - Effect of adsorbed oxygen on the friction for various metals in contact with Ni-Zn ferrite. Exposure, 1000L of oxygen gas; sliding velocity, 3 mm/min; load, 0.05 to 0.2 N; vacuum, 30 nPa; room temperature.

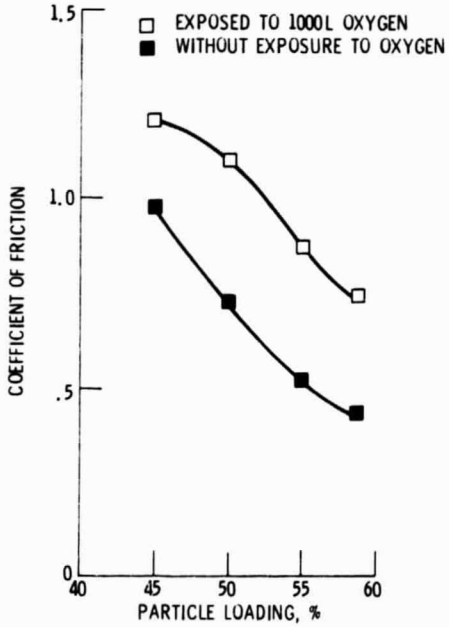

Figure 8. - Coefficients of friction for various magnetic tapes in contact with Ni-Zn ferrite as a function of the particle loading (magnetic particle concentration). Effect of adsorbed oxygen on friction for various tapes. Exposure, 1000 L of oxygen gas; sliding velocity, 3 mm/min; load, 0.5 N; vacuum, 30 nPa; room temperature.

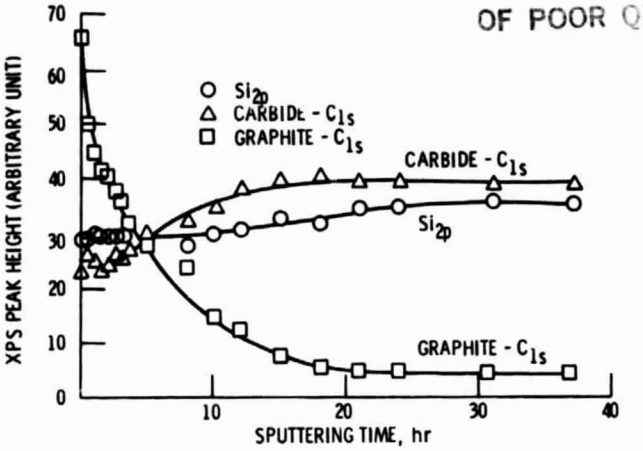

Figure 9. - Elemental depth profile of silicon carbide {0001} surface preheated to a temperature of 1500° C for 1 hour.

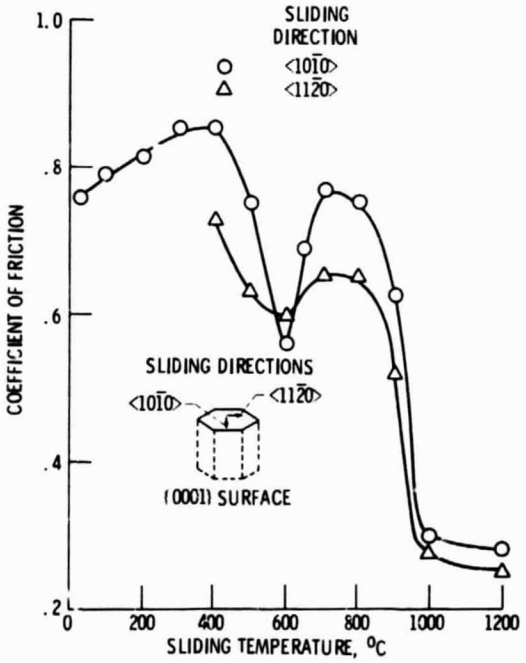

Figure 10. - Effect of temperature on coefficient of friction for silicon carbide {0001} surface sliding against an iron rider. The iron rider was argon ion sputter cleaned before experiments. Normal load, 0.2 N, vacuum, 10 nPa.

(a) ROOM TEMPERATURE.

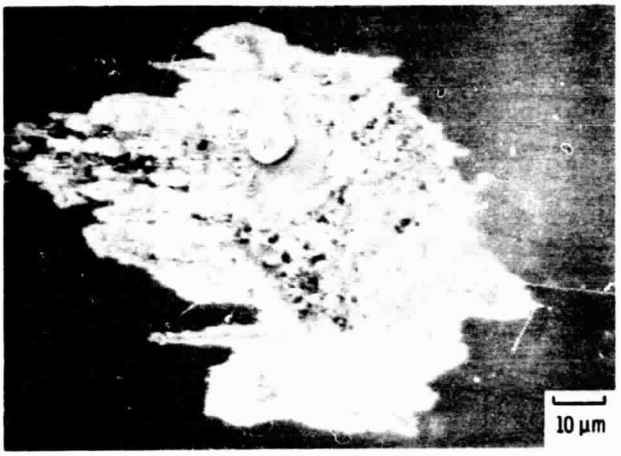

(b) 800° C.

(c) 1200° C.

Figure 11. - Iron transferred to single-crystal silicon carbide at commencement of sliding as a result of single pass of rider at room temperature, 800° C and 1200° C in vacuum. Silicon carbide {0001} surface; sliding direction <1$\bar{0}$10>; load, 0.2 N; vacuum pressure, 10 n Pa.

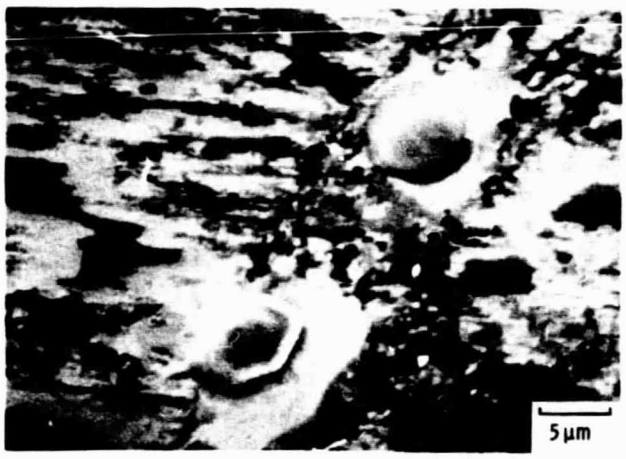

(a) WEAR TRACK.

(b) PIT WITH A SPHERICAL PARTICLE.

(c) PIT WITH A HEXAGONAL SHAPED WEAR DEBRIS.

Figure 12. - Fracture pits with a spherical particle and with a multiangular shaped wear debris. Scanning electron micrographs of wear track on silicon carbide (0001) surface. Single pass sliding of iron rider, load, 0.2 N; temperature, 800°C; vacuum, 10 n Pa.